Vietnam Journal of Mechanics, VAST, Vol. 44, No. 1 (2022), pp. 69 – 81
DOI: https://doi.org/10.15625/0866-7136/16834

SIZE-DEPENDENT BEHAVIOR OF A MEMS MICROBEAM UNDER ELECTROSTATIC ACTUATION

Cong Ich Le[1,*], Quang Dung Tran[1], Van Dung Lam[1], Dinh Kien Nguyen[2,3]
[1]*Le Quy Don Technical University, 236 Hoang Quoc Viet street, Hanoi, Vietnam*
[2]*Graduate University of Science and Technology, VAST, 18 Hoang Quoc Viet street, Hanoi, Vietnam*
[3]*Institute of Mechanics, VAST, 264 Doi Can street, Hanoi, Vietnam*
[*]E-mail: lecongich79@lqdtu.edu.vn

Received: 19 December 2021 / Published online: 31 March 2022

Abstract. The size-dependent behavior of a silicon microbeam with an axial force in MEMS is studied using a nonlinear finite element procedure. Based on a refined third-order shear deformation theory and the modified couple stress theory (MCST), nonlinear differential equations of motion for the beam are derived from Hamilton's principle, and they are transferred to a discretized form using a two-node beam element. Newton-Raphson based iterative procedure is used in conjunction with Newmark method to obtain the pull-in voltages and deflections of a clamped-clamped microbeam under electrostatic actuation. The influence of the axial force, applied voltage and material length scale parameter on the behavior of the beam is studied in detail and highlighted.

Keywords: microbeam, modified couple stress theory, electrostatic actuation, refined third-order shear deformation theory, nonlinear finite element analysis.

1. INTRODUCTION

Microbeams are used in many micro-electromechanical system (MEMS) devices such as capacitive MEMS switches and resonant sensors. Under electric actuation, both the DC and AC voltages, these microbeams often undergo moderately large deflection, and thus nonlinear static and dynamic analysis is required to assess the mechanical behavior of the MEMS microbeams. Both analytical and numerical methods have been developed for studying the response of electrically actuated microbeams.

The classical Euler-Bernoulli beam theory which ignores the size effect has been employed by several authors to study mechanical behavior of MEMS microbeams. The Euler–Bernoulli beam model was used in conjunction with the shooting method by Choi and Lovell [1] in development of a numerical procedure for computing deflections and stresses of a clamped microbeam under mechanical and electrostatic loads. Abdel–

© 2022 Vietnam Academy of Science and Technology

Rahman et al. [2] presented a nonlinear beam model for the electrically actuated microbeams of MEMS. The microbeam in the system is modeled as a distributed-mass structure bending under an electric actuation force and subjected to mid-plane stretching and axial loading. The governing equation was solved by the shooting method for the deflections and frequencies. Younis et al. [3] derived the fourth-order differential equations of motion for an axially loaded MEMS microbeam an electric load and subjected to a viscous damping. With the aid of Galerkin method, the equations are converted to the discrete form, and the static and dynamic pull-in behavior was studied in detail. Younis and Nayfeh [4] employed the perturbation method to obtain the first-order nonlinear differential equations in their nonlinear analysis of a resonant microbeam under an electric actuation and an axial force. The effects of the axial force as well as the DC electrostatic and AC harmonic forces on the dynamic responses were examined. Also using the perturbation method, Abdel–Rahman and Nayfeh [5] studied response of a microbeam-based resonant sensor to super-harmonic and sub-harmonic electric actuations. The frequency-response and force-response curves were obtained for the sensor with clamped ends. Chaterjee and Pohit [6] considered the pull-in problem of electrostatically actuated microcantilever beams with relatively large gap between the microbeam and the stationary electrode. The obtained result reveals that the nonlinearities play a significant role when pull-in occurs. Static and dynamic pull-in behavior of resonant microbeams was considered by Ghazavi et al. [7] using a two-node beam element and the software ANSYS, respectively. Rezazadeh et al. [8] employed the finite difference method to compute pull-in voltage of a fixed-fixed microbeam subjected to electrostatic load. The effect of axial stress on the instability of the microbeam was considered by the authors. The pull-in instability of microcantilever in MEMS devices was investigated by Kaneria et al. [9] with the aid of the COMSOL Multiphysics finite element package.

The influence of size effect on mechanical behavior of MEMS has been taken into consideration recently. Based on the modified couple stress theory (MCST) and Euler–Bernoulli beam theory, Farokhi and Ghayesh [10] derived the governing equation for nonlinear static and dynamic behaviors of microcantilever-based MEMS under an electric excitation. The obtained fourth-order equation was then converted into a reduced-order model of the system, and dynamic response was computed with the aid of arc-length continuation technique. The result of the work revealed that the classical theory overestimated the amplitude of the transverse displacement and predicts the lower static pull-in voltage. Ghayesh and Farokhi [11] considered the electrode of MEMS as a microplate in studying nonlinear behavior of electrically actuated MEMS resonators. The weighted-residual method was used in conjunction with a continuation method coupled with backward differentiation formula to obtain the nonlinear characteristics of the microplate. The influence of the size effect on the nonlinear response of the plate was examined. Baghani [12] presented an analytical method to study the size-dependent static pull-in voltage of microcantilevers of MEMS. The method based on the modified variational iteration procedure enables to assess the nonlinear response of the microbeams under electric actuation. Ghayesh et al. [13] studied nonlinear size-dependent resonant behavior of MEMS resonators, in which the microbeam with an axial force is subjected to both DC and AC voltages. Euler–Bernoulli beam theory and the MCST were adopted to

derive the nonlinear differential equations, and Galerkin method was employed to obtain the frequency-response curves of the system.

In this paper, the size-dependent behavior of a silicon microbeams with an axial force under electostatic actuation of a DC voltage is studied using a nonlinear finite element procedure. Different from above discussed references, the microbeam is modelled by a refined third-order shear deformation theory, in which the transverse displacement is split into bending and shear parts. Based on the MCST, nonlinear governing equations for the microbeam are derived and transferred into a discretized form by a two-node beam element. A Newton–Raphson based iterative procedure is used in conjunction with the Newmark method to compute the response of the microbeam with clamped ends. The effects of the axial force, the applied voltage and the material size parameter on the behavior of the microbeam are studied and highlighted.

2. MATHEMATICAL FORMULATION

A clamped-clamped silicon microbeam with rectangular cross section formed one side of a capacitor [4, 13] as depicted in Fig. 1 is considered. In the figure, L, h, b and d are, respectively, the total length, height, width of the beam and the air-gap between the microbeam and electrode. The Cartesian coordinates (x, y, z) is chosen such that the (x, y) plane is coincident with the beam mid-plane.

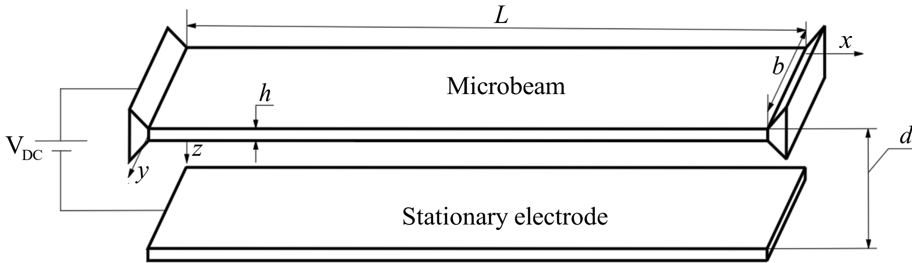

Fig. 1. Model of an electrostatically actuated microbeam in MEMS

Based on the refined third-order shear deformation theory of Shimpi and Patel [14], the axial and transverse displacements of a point in the beam, $u_1(x, z, t)$ and $u_3(x, t)$, respectively, are given by

$$\begin{aligned} u_1(x,z,t) &= u_0(x,t) - z w_{b,x}(x,t) - f(z)\, w_{s,x}(x,t), \\ u_3(x,t) &= w_b(x,t) + w_s(x,t), \end{aligned} \tag{1}$$

where $u_0(x, t)$ is the axial displacement of a point on the mid-plane; $w_b(x, t)$ and $w_s(x, t)$ are, respectively, the bending and shear parts of the transverse displacement; t is the time variable, and the shearing shape function $f(z)$ is of the form

$$f(z) = z\Big[-\frac{1}{4} + \frac{5}{3}\Big(\frac{z}{h}\Big)^2\Big]. \tag{2}$$

In Eq. (1) and hereafter, a subscript comma is used to denote the derivative with respect to the variable that follows, e.g. $w_{b,x} = \partial w_b / \partial x$.

The normal strain (ε_{xx}) and the shear strains (γ_{xz}) based on the von Kármán nonlinear strain-displacement relationship are given by

$$\begin{aligned} \varepsilon_{xx} &= u_{1,x} + \frac{1}{2} u_{3,x}^2 = u_{0,x} - z w_{s,xx} - f(z) w_{s,xx} + \frac{1}{2}(w_{b,x} + w_{s,x})^2, \\ \gamma_{xz} &= u_{1,z} + u_{3,x} = g(z)\, w_{s,x}, \end{aligned} \tag{3}$$

where $g(z) = 1 - f_{,z} = 5\left[\frac{1}{4} - \left(\frac{z}{h}\right)^2\right]$.

The constitutive equation based on linear behavior of the beam material is

$$\sigma_{xx} = E\varepsilon_{xx}, \quad \tau_{xz} = G\gamma_{xz}, \tag{4}$$

where σ_{xx} and τ_{xz} are, respectively, the normal and shear stresses; E, $G = \dfrac{E}{2(1+\nu)}$ and ν are Young's modulus, shear modulus and Poisson's ratio, respectively.

It is well-known that the classical continuum mechanics is not sufficient to predict the size-dependent behavior of micron-scale structures. Several higher order continuum theories, such as the couple stress theory that contains four material constants (two classical and two additional), strain gradient theory, micropolar theory, nonlocal elasticity theory ... have been developed to account for the size effect in the small-scale structures. The MCST proposed by Yang et al. [15] is adopted herein to evaluate the strain energy of the microbeam as

$$\mathcal{U} = \frac{1}{2} \int_V (\boldsymbol{\sigma} : \boldsymbol{\varepsilon} + \boldsymbol{m} : \boldsymbol{\chi}) \mathrm{d}V, \tag{5}$$

where V is the beam volume; $\boldsymbol{\sigma}$ and $\boldsymbol{\varepsilon}$ are, respectively, the stress and strain tensors; $\boldsymbol{m}$ is the deviatoric part of the couple stress tensor and $\boldsymbol{\chi}$ is the symmetric curvature tensor. For the beam under consideration, these tensors are given by

$$\boldsymbol{\sigma} = \begin{bmatrix} \sigma_{xx} & 0 & \tau_{xz} \\ 0 & 0 & 0 \\ \tau_{xz} & 0 & 0 \end{bmatrix}, \ \boldsymbol{\varepsilon} = \begin{bmatrix} \varepsilon_{xx} & 0 & \gamma_{xz}/2 \\ 0 & 0 & 0 \\ \gamma_{xz}/2 & 0 & 0 \end{bmatrix}, \ \boldsymbol{\chi} = \begin{bmatrix} 0 & \chi_{xy} & 0 \\ \chi_{xy} & 0 & 0 \\ 0 & 0 & 0 \end{bmatrix}, \ \boldsymbol{m} = 2l^2 G \boldsymbol{\chi}, \tag{6}$$

where $\chi_{xy} = -(w_{b,xx} + w_{s,xx})/2 + g(z) w_{s,xx}/4;\ m_{xy} = 2Gl^2 \chi_{xy}$, and l is the material length scale parameter. Using Eq. (6), one can rewrite the strain energy of the beam in Eq. (5) in the form

$$\mathcal{U} = \frac{b}{2} \int_0^L \int_{-h/2}^{h/2} (\sigma_{xx}\varepsilon_{xx} + \tau_{xz}\gamma_{xz} + 2m_{xy}\chi_{xy}) \mathrm{d}z\mathrm{d}x. \tag{7}$$

The kinetic energy of the beam resulted from Eq. (1) is of the form

$$\mathcal{T} = \frac{\rho}{2} \int_V (\dot{u}_1^2 + \dot{u}_3^2) \mathrm{d}V = \frac{\rho\, b}{2} \int_0^L \int_{-h/2}^{h/2} [(\dot{u}_0 - z\, \dot{w}_{b,x} - f(z)\, \dot{w}_{s,x})^2 + (\dot{w}_b + \dot{w}_s)^2] \mathrm{d}z\mathrm{d}x, \tag{8}$$

where ρ is the mass density, and an over dot denotes the derivative with respect to the time variable t.

The beam is exerted by the electrostatic force per unit length in the form [10,13]

$$q(x,t) = \frac{\varepsilon_0 b {\mathrm{V}_{\mathrm{DC}}}^2}{2(d - u_3(x,t))^2}, \tag{9}$$

where V_{DC} is the DC polarization voltage, and ε_0 is the dielectric constant of vacuum. The beam is also assumed to be subjected to viscous damping of coefficient c_0.

The potential energy $(\mathcal{V}_E)$ of the electrostatic force in Eq (9) is given by [16]

$$\mathcal{V}_E = -\frac{1}{2}\int_0^L \frac{\varepsilon_0 b {\mathrm{V}_{\mathrm{DC}}}^2}{2(d - u_3)}\,\mathrm{d}x. \tag{10}$$

In addition, the microbeam is assumed to be under action of an axial force P, which results in energy $\mathcal{U}_P$ of the form

$$\mathcal{U}_P = \frac{P}{2}\int_0^L u_{3,x}^2 \mathrm{d}x = \frac{P}{2}\int_0^L (w_{b,x} + w_{s,x})^2 \mathrm{d}x. \tag{11}$$

The damping mechanism is formulated herein by using the Rayleigh dissipation function $\mathcal{D}$ as follows

$$\mathcal{D} = \frac{c_0}{2}\int_0^L [\dot{u}_0^2 + (\dot{w}_b + \dot{w}_s)^2]\mathrm{d}x, \tag{12}$$

where c_0 is the coefficient of the viscous damping.

Equations of motion for the microbeam can be derived from Hamilton's principle, which can be expressed as

$$\delta\int_{t_1}^{t_2} [\mathcal{T} - (\mathcal{U}_b + \mathcal{U}_P + \mathcal{V}_E + \mathcal{D})] = 0. \tag{13}$$

Substituting Eqs. (7)–(12) into Eq. (13) one can obtain the following nonlinear partial differential equations of motion for the microbeam

$$\rho A \ddot{u}_0 + c_0 \dot{u}_0 - \frac{EA}{2}\left(2u_{0,xx} + w_{b,x}w_{b,xx} + w_{b,xx}w_{s,x} + w_{b,x}w_{s,xx} + w_{s,x}w_{s,xx}\right) = 0, \tag{14}$$

$$\begin{aligned}
&\rho A(\ddot{w}_b + \ddot{w}_s) - \rho I \ddot{w}_{b,xx} + c_0(\dot{w}_b + \dot{w}_s) + EI w_{b,xxxx} - \frac{3EA}{8}\Big(w_{b,xx}w_{b,x}^2 \\
&+ 2w_{b,x}w_{b,xx}w_{s,x} + w_{b,x}^2 w_{s,xx} + 2w_{b,x}w_{s,x}w_{s,xx} + w_{s,x}^2 w_{b,xx} + w_{s,xx}w_{s,x}^2\Big) \\
&- \frac{EA}{2}\Big(u_{0,xx}w_{b,x} + u_{0,x}w_{b,xx} + u_{0,xx}w_{s,x} + u_{0,x}w_{s,xx}\Big) \\
&+ GAl^2\Big(w_{b,xxx} + \frac{7}{12}w_{s,xxx}\Big) - P(w_{b,xx} + w_{s,xx}) = \frac{\varepsilon_0\, b\, \mathrm{V}_{DC}^2}{2(d - w_b - w_s)^2},
\end{aligned} \tag{15}$$

$$
\begin{aligned}
&\rho A(\ddot{w}_b+\ddot{w}_s)-\frac{\rho I}{84}\ddot{w}_{s,xx}+c_0(\dot{w}_b+\dot{w}_s)+\frac{EI}{84}w_{s,xxxx}-\frac{3EA}{8}\Big(w_{b,xx}w_{b,x}^2\\
&+2w_{s,x}w_{s,xx}w_{b,x}+w_{b,x}^2w_{s,xx}+2w_{b,x}w_{b,xx}w_{s,x}+w_{s,x}^2w_{b,xx}+w_{s,xx}w_{s,x}^2\Big)\\
&-\frac{EA}{2}\Big(u_{0,xx}w_{b,x}+u_{0,x}w_{b,xx}+u_{0,xx}w_{s,x}+u_{0,x}w_{s,xx}\Big)-\frac{GA}{2}\Big(\frac{5}{3}w_{s,xx}\\
&-7l^2\,w_{b,xxxx}-\frac{3l^2}{4}w_{s,xxxx}\Big)-P(w_{b,xx}+w_{s,xx})=\frac{\varepsilon_0\,b\,V_{DC}^2}{2(d-w_b-w_s)^2}.
\end{aligned}
\tag{16}
$$

In the above equations, $A=(b\times h)$ and $I=bh^3/12$ are, respectively, the cross-sectional area and the second moment of inertia of the beam cross section. The constraints for both the clamped ends are $u_0=w_b=w_s=w_{b,x}=w_{s,x}=0$ at $x=0$ and $x=L$.

Derivation of a closed-formed solution for the system of nonlinear equations (14)–(16) is cumbersome. The finite element method is employed herein to solve the nonlinear differential equations.

3. SOLUTION METHOD

A finite element formulation is formulated in this Section to transfer the nonlinear differential equations (14)–(16) into a discretized form. To this end, the beam is assumed to be divided into a number of two-node beam elements with length of l_e. The vector of nodal displacements $(\mathbf{q}_e)$ for an element contains ten components as

$$
\mathbf{q}_e=\{\mathbf{u}_0,\ \mathbf{w}_b,\ \mathbf{w}_s\}^T,
\tag{17}
$$

where

$$
\mathbf{u}_0=\{u_{01},u_{02}\}^T,\ \mathbf{w}_b=\{w_{b1},\ w_{b1,x},\ w_{b2},\ w_{b2,x}\}^T,\ \mathbf{w}_s=\{w_{s1},\ w_{s1,x},\ w_{s2},\ w_{s2,x}\}^T,
\tag{18}
$$

are, respectively, the vectors of nodal axial displacements, bending and shear transverse displacements. The displacements inside the element are interpolated from the nodal values according to

$$
u_0=\mathbf{N}\mathbf{u}_0,\ \ w_b=\mathbf{H}\mathbf{w}_b,\ \ w_s=\mathbf{H}\mathbf{w}_s,
\tag{19}
$$

where $\mathbf{N}=[N_1,\ N_2]$ and $\mathbf{H}=[H_1,\ H_2,\ H_3,\ H_4]$ are the matrices of the interpolating functions. The following linear and Hermite functions used in [17] are adopted for the functions N_i $(i=1,2)$ and H_j $(j=1,\dots,4)$

$$
N_1=\frac{l_e-x}{l_e},\quad N_2=\frac{x}{l_e},
\tag{20}
$$

and

$$
H_1=1-\frac{3x^2}{l_e^2}+\frac{2x^3}{l_e^3},\ H_2=x-\frac{2x^2}{l_e}+\frac{x^3}{l_e^2},\ H_3=\frac{3x^2}{l_e^2}-\frac{2x^3}{l_e^3},\ H_4=-\frac{x^2}{l_e}+\frac{x^3}{l_e^2},
\tag{21}
$$

Substituting Eq. (19) into Eqs. (14)–(16) and taking integration over the beam length lead to the following matrix-form Galerkin residual equation [18]

$$
\sum^{\mathrm{NE}}\Big(\mathbf{m}_e\ddot{\mathbf{q}}_e+\mathbf{c}_e\dot{\mathbf{q}}_e+\mathbf{k}_e\mathbf{q}_e-\mathbf{f}_e\Big)=0,
\tag{22}
$$

where NE is the total number of elements used to discretize the beam; $\mathbf{m}_e$, $\mathbf{c}_e$ and $\mathbf{k}_e$ are, respectively, the element mass, damping and stiffness matrices; $\mathbf{f}_e$, $\dot{\mathbf{q}}_e$ and $\ddot{\mathbf{q}}_e$ are the element vectors of the nodal force, nodal velocities and nodal accelerations, respectively. The matrices in Eq. (22) can be written in sub-matrix forms as follows

$$\underset{10\times10}{\mathbf{m}_e} = \begin{bmatrix} \mathbf{m}_{aa} & \mathbf{0} & \mathbf{0} \\ \mathbf{0}^T & \mathbf{m}_{bb} & \mathbf{m}_{bs} \\ \mathbf{0}^T & \mathbf{m}_{bs}^T & \mathbf{m}_{ss} \end{bmatrix}, \quad \underset{10\times10}{\mathbf{c}_e} = \begin{bmatrix} \mathbf{c}_{aa} & \mathbf{0} & \mathbf{0} \\ \mathbf{0}^T & \mathbf{c}_{bb} & \mathbf{c}_{bs} \\ \mathbf{0}^T & \mathbf{c}_{bs}^T & \mathbf{c}_{ss} \end{bmatrix}, \quad \underset{10\times10}{\mathbf{k}_e} = \begin{bmatrix} \mathbf{k}_{aa} & \mathbf{k}_{ab} & \mathbf{k}_{as} \\ \mathbf{k}_{ab}^T & \mathbf{k}_{bb} & \mathbf{k}_{bs} \\ \mathbf{k}_{as}^T & \mathbf{k}_{bs}^T & \mathbf{k}_{ss} \end{bmatrix}. \tag{23}$$

The element nodal force vector has the form

$$\underset{10\times1}{\mathbf{f}_e} = \left\{\mathbf{0}, \quad \mathbf{f}_b, \quad \mathbf{f}_s\right\}^T. \tag{24}$$

In the above equations, the subscripts 'a', 'b' and 's' stand for the 'axial', 'bending' and 'shear', respectively. The detail expressions for the sub-matrices and sub-vector in Eqs. (23) and (24) are as follows

$$\begin{aligned} \underset{(2\times2)}{\mathbf{m}_{aa}} &= \int_0^{l_e} \mathbf{N}^T \rho A \mathbf{N} \mathrm{d}x, \quad \underset{(4\times4)}{\mathbf{m}_{bb}} = \rho A \int_0^{l_e} \mathbf{H}^T \mathbf{H} \mathrm{d}x + \rho I \int_0^{l_e} \mathbf{H}_{,x}^T \mathbf{H}_{,x} \mathrm{d}x, \\ \underset{(4\times4)}{\mathbf{m}_{bs}} &= \rho A \int_0^{l_e} \mathbf{H}^T \mathbf{H} \mathrm{d}x, \quad \underset{(4\times4)}{\mathbf{m}_{ss}} = \rho A \int_0^{l_e} \mathbf{H}^T \mathbf{H} \mathrm{d}x + \rho I \int_0^{l_e} \mathbf{H}_{,x}^T \mathbf{H}_{,x} \mathrm{d}x, \end{aligned} \tag{25}$$

$$\underset{(2\times2)}{\mathbf{c}_{aa}} = c_0 \int_0^{l_e} \mathbf{N}^T \mathbf{N} \mathrm{d}x, \quad \underset{(4\times4)}{\mathbf{c}_{bb}} = c_0 \int_0^{l_e} \mathbf{H}^T \mathbf{H} \mathrm{d}x, \quad \underset{(4\times4)}{\mathbf{c}_{bs}} = \underset{(4\times4)}{\mathbf{c}_{ss}} = \underset{(4\times4)}{\mathbf{c}_{bb}}, \tag{26}$$

$$\begin{aligned} \underset{(2\times2)}{\mathbf{k}_{aa}} &= EA \int_0^{l_e} \mathbf{N}_{,x}^T \mathbf{N}_{,x} \mathrm{d}x, \quad \underset{(2\times4)}{\mathbf{k}_{ab}} = \frac{EA}{2} \int_0^{l_e} \mathbf{N}_{,x}^T (w_{b,x} + w_{s,x}) \mathbf{H}_{,x} \mathrm{d}x, \quad \mathbf{k}_{as} = \mathbf{k}_{ab}, \\ \underset{(4\times4)}{\mathbf{k}_{bb}} &= AE \int_0^{l_e} \Big(\frac{3}{8} \mathbf{H}_{,x}^T (w_{b,x}^2 + w_{s,x}^2) \mathbf{H}_{,x} + \frac{3}{4} \mathbf{H}_{,x}^T (w_{b,x} w_{s,x}) \mathbf{H}_{,x} \Big) \mathrm{d}x \\ &\quad + P \int_0^{l_e} \mathbf{H}_{,x}^T \mathbf{H}_{,x} \mathrm{d}x + EI \int_0^{l_e} \mathbf{H}_{,xx}^T \mathbf{H}_{,xx} \mathrm{d}x \\ &\quad + AE \int_0^{l_e} \Big(\frac{1}{2} \mathbf{H}_{,x}^T (u_{0,x}) \mathbf{H}_{,x} + \frac{7l^2}{24(1+\nu)} \mathbf{H}_{,xx}^T \mathbf{H}_{,xx} \Big) \mathrm{d}x + P \int_0^{l_e} \mathbf{H}_{,x}^T \mathbf{H}_{,x} \mathrm{d}x, \\ \underset{(4\times4)}{\mathbf{k}_{bs}} &= AE \int_0^{l_e} \Big(\frac{3}{8} \mathbf{H}_{,x}^T (w_{b,x}^2 + w_{s,x}^2) \mathbf{H}_{,x} + \frac{3}{4} \mathbf{H}_{,x}^T (w_{b,x} w_{s,x}) \mathbf{H}_{,x} \\ &\quad + \frac{1}{2} \mathbf{H}_{,x}^T (u_{0,x}) \mathbf{H}_{,x} + \frac{7l^2}{24(1+\nu)} \mathbf{H}_{,xx}^T \mathbf{H}_{,xx} \Big) \mathrm{d}x, \\ \underset{(4\times4)}{\mathbf{k}_{ss}} &= EA \int_0^{l_e} \Big(\frac{3}{8} \mathbf{H}_{,x}^T (w_{b,x}^2 + w_{s,x}^2) \mathbf{H}_{,x} + \frac{3}{4} \mathbf{H}_{,x}^T (w_{b,x} w_{s,x}) \mathbf{H}_{,x} + \frac{1}{2} \mathbf{H}_{,x}^T (u_{0,x}) \mathbf{H}_{,x} \\ &\quad + \frac{3l^2}{16(1+\nu)} \mathbf{H}_{,xx}^T \mathbf{H}_{,xx} \Big) \mathrm{d}x + \frac{EI}{84} \int_0^{l_e} \mathbf{H}_{,xx}^T \mathbf{H}_{,xx} \mathrm{d}x + P \int_0^{l_e} \mathbf{H}_{,x}^T \mathbf{H}_{,x} \mathrm{d}x, \end{aligned} \tag{27}$$

and

$$\underset{(4\times1)}{\mathbf{f}_b} = \underset{(4\times1)}{\mathbf{f}_s} = \int_0^{l_e} q(x,t)\mathbf{H}^T \mathrm{d}x. \tag{28}$$

Since the highest order of the polynomials under the integrals in Eqs. (25)–(28) is eight, thus the integrals can be exactly evaluated by five Gauss points.

After assembling the element matrices and force vector, once can construct the discrete nonlinear equation of motion for the microbeam in the form

$$\mathbf{M}\ddot{\mathbf{D}} + \mathbf{C}\dot{\mathbf{D}} + \mathbf{K}\mathbf{D} - \mathbf{F} = 0, \tag{29}$$

where **M**, **C**, **K** and **F** are, respectively, the global mass, damping, stiffness matrices and global force vector; **D**, $\dot{\mathbf{D}}$ and $\ddot{\mathbf{D}}$ are the global vectors of nodal displacements, nodal velocities and nodal accelerations, respectively. A Newton–Raphson based iterative procedure is used in combination with Newmark method to solve Eq. (29). In case of static analysis, both $\dot{\mathbf{D}}$ and $\ddot{\mathbf{D}}$ are set to zeros, and only the iterative procedure is used to compute **D**.

4. NUMERICAL RESULTS AND DISCUSSION

Numerical investigation is carried out in this section to highlight the effects of various factors such as the axial force, the applied voltage and the beam properties on behavior of the microbeam. The microbeam is discretized herewith by 20 elements for all computations below. For the convenience of discussion, the following dimensionless parameters are introduced

$$\begin{aligned} &\mu = \omega_1\sqrt{\frac{\rho A L^4}{EI}},\ N^* = \frac{PL^2}{EI},\ W_{\max} = \max\left(\frac{u_3}{d}\right),\ \eta = \frac{l^2 AG}{EI},\\ &\text{and}\quad \alpha_1 = 6\left(\frac{d}{h}\right)^2,\ \alpha_2 = \frac{6\varepsilon_0 L^4}{Eh^3 d^3}, \end{aligned} \tag{30}$$

with ω_1 is the fundamental frequency of the microbeam.

The derived formulation is necessary to verify before computing the response of the microbeam. To this end, Tables 1 and 2 compare the static and dynamic pull-in voltages obtained by present formulation with that of Refs. [7,8,19]. A good agreement between the present result with that of the cited references can be noted from the tables, regardless of the beam length, the air gap, the axial force and the damping coefficient as well. Noting that the finite element method is used in Ref. [7], while the finite difference method and the 3D MEMCAD model were employed in Refs. [8,19], respectively.

In Fig. 2, the frequency parameter μ versus the V_{DC} voltage is depicted for $\eta = 0$ and various values of the axial forces, where for comparison purpose, the result obtained by Galerkin method of Ref. [20] is also given. The curves for the frequency parameter μ versus the V_{DC} voltage with different material length scales η are shown in Fig. 3. Both Figs. 2 and 3 were obtained for the beam with $L = 210$ µm, $b = 100$ µm, $h = 1.5$ µm, $d = 1.18$ µm, $\nu = 0.06$ and $E = 169$ GPa [20]. Fig. 2 confirms the accuracy of the present formulation in evaluating the frequency of the beam, and it also shows the important role of the axial force on the frequency and pull-in voltage. Both the frequency and the pull-in

Table 1. Comparison of static pull-in voltages for $E = 169$ GPa, $\nu = 0.06$, $b = 50$ µm, $h = 3$ µm, $\eta = 0$ and different values of L (µm), d (µm) and P with P/A (MPa)

Beam properties			$V_{\text{pull-in}}$				Error (%)
L	d	P/A	Ref. [7]	Ref. [8]	Ref. [19]	Present	
250	1	0	39.60	39.13	39.50	39.60	0/1.19/0.25
250	1	100	58.30	58.84	56.90	58.33	0.05/0.87/2.51
250	1	−25	33.10	33.04	33.70	33.07	0.09/0.08/1.87
350	1	0	-*	20.36	20.30	20.27	-/0.45/0.15
350	1	100	-	36.99	35.40	36.47	-/1.42/3.02
350	1	−25	-	13.27	13.80	12.93	-/2.56/6.30
250	2	0	113.30	-	-	114.20	0.79/-/-
250	2	100	165.60	-	-	166.50	0.54/-/-
250	2	−25	96.20	-	-	96.60	0.42/-/-
250	3	0	215.70	-	-	217.60	0.88/-/-
250	3	100	307.50	-	-	309.80	0.75/-/-
250	3	−25	185.30	-	-	186.60	0.70/-/-
350	0.5	0	-	7.07	-	7.12	-/0.71/-
350	2	0	-	57.59	-	58.30	-/1.23/-

Note: * not available.

Table 2. Comparison of dynamic pull-in voltage for $L = 250$ µm, $b = 50$ µm, $h = 3$ µm, $E = 169$ GPa, $\nu = 0.06$, $\eta = 0$ and various values of d, c_0 and P

Sources	d	$P/A = 0$			$P/A = -25$			$P/A = 100$		
		$c_0 = 0.4$	$c_0 = 0.8$	$c_0 = 1.6$	$c_0 = 0.325$	$c_0 = 0.65$	$c_0 = 1.3$	$c_0 = 0.55$	$c_0 = 1.1$	$c_0 = 2.2$
Ref. [7]	1	38.80	39.40	39.60	32.30	33.00	33.10	56.80	58.10	58.30
Present		38.71	39.63	39.59	32.34	33.12	33.10	56.80	58.29	58.31
Ref. [7]	2	110.40	111.70	113.30	93.20	95.60	96.20	160.60	164.10	165.60
Present		111.68	114.18	114.19	94.20	96.40	96.40	161.89	166.25	166.30
Ref. [7]	3	208.60	212.90	215.70	178.10	182.50	185.30	296.40	303.80	307.50
Present		212.26	217.16	217.19	181.98	186.53	186.57	301.73	309.77	309.92

voltage are decreased of the compressive axial force amplitude, while they are increased by the tensile axial force. The material length scale parameter, as seen from Fig. 3, has an important role on both the frequency and pull-in voltage, and both these quantities are considerably underestimated by ignoring the size effect.

The effects of the material length scale and the axial force on the nonlinear bending behavior of the microbeam are shown in Figs. 4 and 5, respectively. In Fig. 4, for the comparison purpose, the available result of Ghayesh et al. [13] is also shown given. In addition to the excellent agreement between the present result with that of Ref. [13], the figures also show the important role of the material length scale and the axial force on the

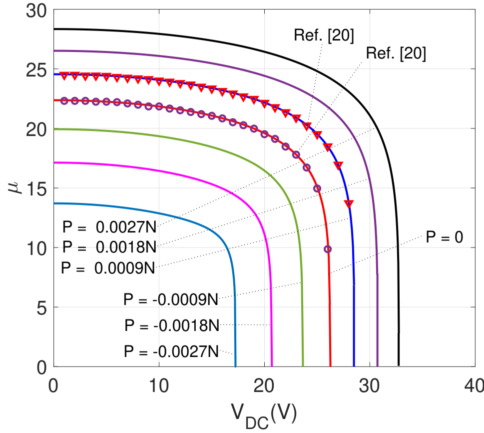

Fig. 2. Frequency parameter μ versus applied voltage $\mathrm{V_{DC}}$ for $\eta = 0.$ and various values of P

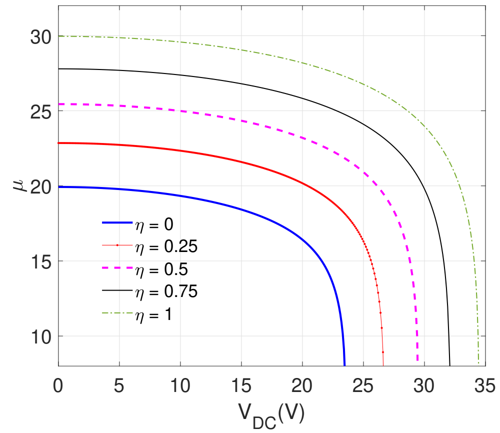

Fig. 3. Frequency parameter μ versus applied voltage $\mathrm{V_{DC}}$ for $P = -0.0009$ N and different η

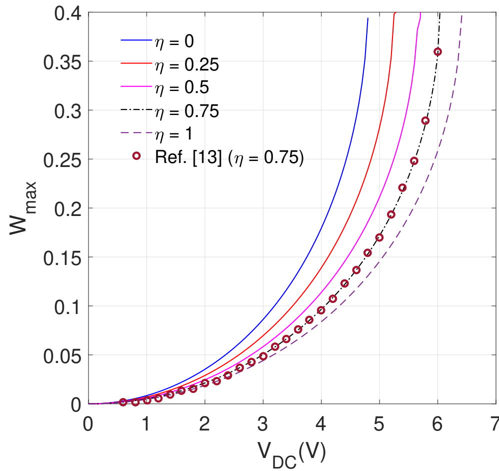

Fig. 4. Effect of scale parameter η on relation between maximum deflection with applied voltage for $\alpha_1 = 3.71, \alpha_2 = 3.9, N^* = 8.7, \nu = 0.06$

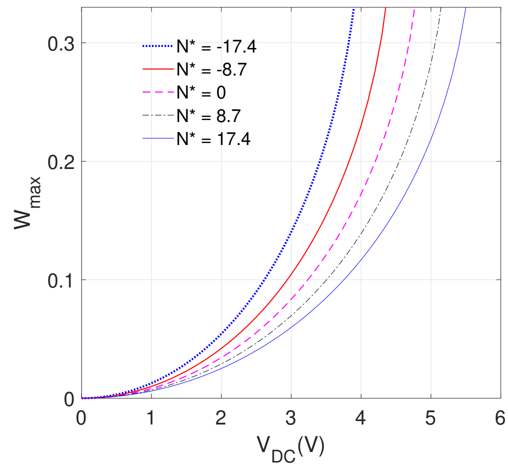

Fig. 5. Effect of axial force on relation between maximum deflection with applied voltage for $\alpha_1 = 3.71, \alpha_2 = 3.9, \nu = 0.06, \eta = 0.25$

nonlinear bending of the beam. At a given value of the $\mathrm{V_{DC}}$ voltage, the maximum transverse deflection decreases by increasing the material length scale and the axial forces.

Finally, the relations between the maximum deflection $W_{\max}$ and the applied voltage $\mathrm{V_{DC}}$ with the time are shown in Figs. 6 and 7, respectively. The curves in the figures are obtained for $L = 250$ µm, $b = 50$ µm, $h = 3$ µm, $d = 1$ µm, $E = 169$ GPa, $\nu = 0.06$, $\eta = 0.5$, and $c_0 = 1.6$ kg/s.m (as in Refs. [7,8,20]) ($N^* = 0$ in Fig. 6 and various values of N^* in Fig. 7). As seen from Fig. 6, the time necessary for the deflection to attain the

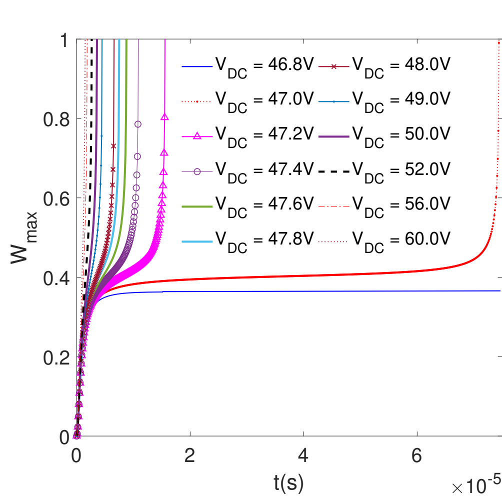

Fig. 6. Maximum deflection $W_{\max}$ versus time for different values of applied voltage V_{DC}

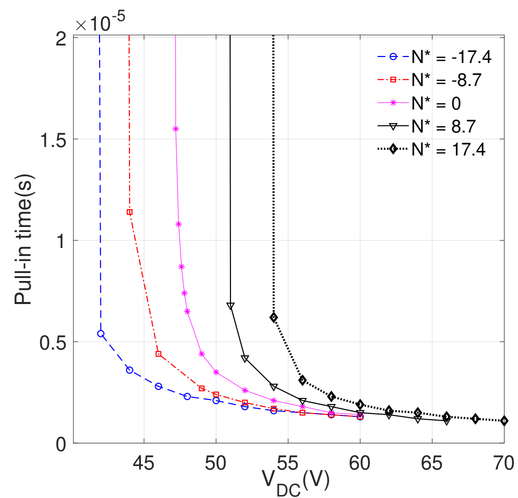

Fig. 7. Pull-in time versus applied voltage V_{DC} for different values of N^*

maximum value decreases by increase of the applied voltage. The time necessary for the deflection to achieve a maximum value when the applied voltage exceeds a certain value, namely $V_{DC} \geq 47.2$ V, is considerably short. The influence of the pull-in time, as seen from Fig. 7, is much dependent on the axial force, and the time necessary for pull-in to occur is decreased by increase of the compressive axial force, but it increases by increasing the tensile axial force.

5. CONCLUSIONS

The size-dependent behavior of a clamped-clamped microbeam with an axial force in MEMS has been studied using a nonlinear finite element procedure. Equations of motion based on the MCST and refined third-order shear deformation theory were derived and transferred to a discretized form using a two-node beam element. The Newton–Raphson iterative procedure was employed in conjunction with Newmark method to compute frequencies, defections, pull-in voltages and pull-in times of the microbeam. Numerical results reveal that the axial force and the material length scale play an important role on the behavior of the beam, and the fundamental frequencies and pull-in voltage are considerably underestimated by ignoring the size effect. A parametric study has been carried out to highlight the influence of the axial force, the material length scale on the nonlinear behavior of the beam.

REFERENCES

[1] B. Choi and E. G. Lovell. Improved analysis of microbeams under mechanical and electrostatic loads. *Journal of Micromechanics and Microengineering*, **7**, (1), (1997). https://doi.org/10.1088/0960-1317/7/1/005.

[2] E. Abdel-Rahman, M. Younis, and A. Nayfeh. Characterization of the mechanical behavior of an electrically actuated microbeam. *Journal of Micromechanics and Microengineering*, **12**, (6), (2002). https://doi.org/10.1088/0960-1317/12/6/306.

[3] M. I. Younis, E. M. Abdel-Rahman, and A. Nayfeh. A reduced-order model for electrically actuated microbeam-based MEMS. *Journal of Microelectromechanical Systems*, **12**, (5), (2003), pp. 672–680. https://doi.org/10.1109/jmems.2003.818069.

[4] M. I. Younis and A. H. Nayfeh. A study of the nonlinear response of a resonant microbeam to an electric actuation. *Nonlinear Dynamics*, **31**, (1), (2003), pp. 91–117. https://doi.org/10.1023/A:1022103118330.

[5] E. M. Abdel-Rahman and A. H. Nayfeh. Secondary resonances of electrically actuated resonant microsensors. *Journal of Micromechanics and Microengineering*, **13**, (3), (2003). https://doi.org/10.1088/0960-1317/13/3/320.

[6] S. Chaterjee and G. Pohit. A large deflection model for the pull-in analysis of electrostatically actuated microcantilever beams. *Journal of Sound and Vibration*, **322**, (4-5), (2009), pp. 969–986. https://doi.org/10.1016/j.jsv.2008.11.046.

[7] M. R. Ghazavi, G. Rezazadeh, and S. Azizi. Finite element analysis of static and dynamic pull-in instability of a fixed-fixed micro beam considering damping effects. *Sensors & Transducers*, **103**, (4), (2009).

[8] G. Rezazadeh, H. Sadeghian, I. Hosseinzadeh, and A. Toloei. Investigation of pull-in phenomenon on extensible micro beam subjected to electrostatic pressure. *Sensors & Transducers Journal*, **79**, (5), (2007), pp. 1173–1179.

[9] A. J. Kaneria, D. S. Sharma, and R. R. Trivedi. Static analysis of electrostatically actuated micro cantilever beam. *Procedia Engineering*, **51**, (2013), pp. 776–780. https://doi.org/10.1016/j.proeng.2013.01.111.

[10] H. Farokhi and M. H. Ghayesh. Size-dependent behaviour of electrically actuated microcantilever-based MEMS. *International Journal of Mechanics and Materials in Design*, **12**, (3), (2016), pp. 301–315.

[11] M. H. Ghayesh and H. Farokhi. Nonlinear behaviour of electrically actuated microplate-based MEMS resonators. *Mechanical Systems and Signal Processing*, **109**, (2018), pp. 220–234. https://doi.org/10.1016/j.ymssp.2017.11.043.

[12] M. Baghani. Analytical study on size-dependent static pull-in voltage of microcantilevers using the modified couple stress theory. *International Journal of Engineering Science*, **54**, (2012), pp. 99–105. https://doi.org/10.1016/j.ijengsci.2012.01.001.

[13] M. H. Ghayesh, H. Farokhi, and M. Amabili. Nonlinear behaviour of electrically actuated MEMS resonators. *International Journal of Engineering Science*, **71**, (2013), pp. 137–155. https://doi.org/10.1016/j.ijengsci.2013.05.006.

[14] R. P. Shimpi and H. G. Patel. Free vibrations of plate using two variable refined plate theory. *Journal of Sound and Vibration*, **296**, (4-5), (2006), pp. 979–999. https://doi.org/10.1016/j.jsv.2006.03.030.

[15] F. A. C. M. Yang, A. C. M. Chong, D. C. C. Lam, and P. Tong. Couple stress based strain gradient theory for elasticity. *International Journal of Solids and Structures*, **39**, (10), (2002), pp. 2731–2743. https://doi.org/10.1016/s0020-7683(02)00152-x.

[16] Y.-C. Hu, C. M. Chang, and S. C. Huang. Some design considerations on the electrostatically actuated microstructures. *Sensors and Actuators A: Physical*, **112**, (1), (2004), pp. 155–161. https://doi.org/10.1016/j.sna.2003.12.012.

[17] C. I. Le, N. A. T. Le, and D. K. Nguyen. Free vibration and buckling of bidirectional functionally graded sandwich beams using an enriched third-order shear deformation beam element. *Composite Structures*, **261**, (2021). https://doi.org/10.1016/j.compstruct.2020.113309.
[18] R. D. Cook. *Concepts and applications of finite element analysis*. John Wiley & Sons, (2002).
[19] P. M. Osterberg and S. D. Senturia. M-TEST: a test chip for MEMS material property measurement using electrostatically actuated test structures. *Journal of Microelectromechanical systems*, **6**, (2), (1997), pp. 107–118. https://doi.org/10.1109/84.585788.
[20] M. I. Younis. *MEMS linear and nonlinear statics and dynamics*. Springer Science & Business Media, Vol. 20, (2011). https://doi.org/10.1007/978-1-4419-6020-7.